Pumice Raft Detection Using Machine-Learning on Multispectral Satellite Imagery

frontiers | Frontiers in Earth Science

BRIEF RESEARCH REPORT
published: 28 April 2022
doi: 10.3389/feart.2022.838532

Pumice Raft Detection Using Machine-Learning on Multispectral Satellite Imagery

Maggie Zheng[1], Tushar Mittal[1]*, Kristen E. Fauria[2], Ajit Subramaniam[3] and Martin Jutzeler[4]*

[1]Department of Earth, Atmospheric and Planetary Sciences, Massachusetts Institute of Technology, Cambridge, MA, United States, [2]Department of Earth and Environmental Sciences, Vanderbilt University, Nashville, TN, United States, [3]Lamont-Doherty Earth Observatory, Columbia University, Palisades, NY, United States, [4]Centre for Ore Deposit and Earth Sciences (CODES), University of Tasmania, Hobart, TAS, Australia

Most of Earth's volcanic eruptions occur underwater, and these submarine eruptions can significantly impact large-scale Earth systems (e.g., enhancing local primary production by phytoplankton). However, detecting submarine eruptions is challenging due to their remote locations, short eruption durations, lack of sea surface signature (if eruptions do not breach the surface), and the transient nature of the surface manifestations of an eruption (e.g., floating pumice clasts, hydrothermal fluids). We can utilize global satellite imagery of 10–30 m resolution (e.g., Landsat 8, Sentinel-2) to detect new eruptions; however, the large data volumes make it challenging to systematically analyze satellite imagery globally. In this study, we address these challenges by developing a new semi-automated analysis framework to detect submarine eruptions through supervised classification of satellite images on Google Earth Engine. We train our algorithm using images from rafts produced by the August 2019 eruption of Volcano F in the Tofua Arc and present a case study using our methodology on satellite imagery from the Rabaul caldera region in Papua New Guinea. We potentially find a large number of new unreported pumice rafts (in ~16% of images from 2017–present). After analysis of the spatial pattern of raft sightings and ancillary geophysical and visual observations, we interpret that these rafts are not the result of a new eruption. Instead, we posit that the observed rafts represent remobilization of pumice clasts from previous historical eruptions. This novel process of raft remobilization may be common at near-shore/partially submarine caldera systems (e.g., Rabaul, Krakatau) and may have significant implications for new submarine eruption detection and volcanic stratigraphy.

Keywords: submarine volcano monitoring, pumice raft dispersal, machine learning (ML), sentinel-2, Google Earth engine (GEE)

OPEN ACCESS

Edited by:
Max Rudolph,
University of California, Davis, United States

Reviewed by:
Simon Carn,
Michigan Technological University, United States
Scott Edward Bryan,
Queensland University of Technology, Australia

****Correspondence:***
Maggie Zheng
mzhengxi@mit.edu
Tushar Mittal
tmittal2@mit.edu

Specialty section:
This article was submitted to Volcanology, a section of the journal Frontiers in Earth Science

Received: *17 December 2021*
Accepted: *04 April 2022*
Published: *28 April 2022*

Citation:
Zheng M, Mittal T, Fauria KE, Subramaniam A and Jutzeler M (2022) Pumice Raft Detection Using Machine-Learning on Multispectral Satellite Imagery. Front. Earth Sci. 10:838532. doi: 10.3389/feart.2022.838532

1 INTRODUCTION

Submarine volcanism is an important driver for Earth's climate and geochemical cycles on global scales (mid-ocean ridge volcanic system and submarine large igneous provinces) as well as on regional scales (Embley et al., 2004; Santana-Casiano et al., 2013; Tilstone et al., 2014; Kelley, 2017; Mittal and Delbridge, 2019). For instance, submarine eruptions inject ash, pumice, and magmatic volatiles (with nutrients such as Fe) into the water column and the atmosphere (White et al., 2015). Pumice rafts, one of the key signatures of some submarine eruptions, can transport volcanic products

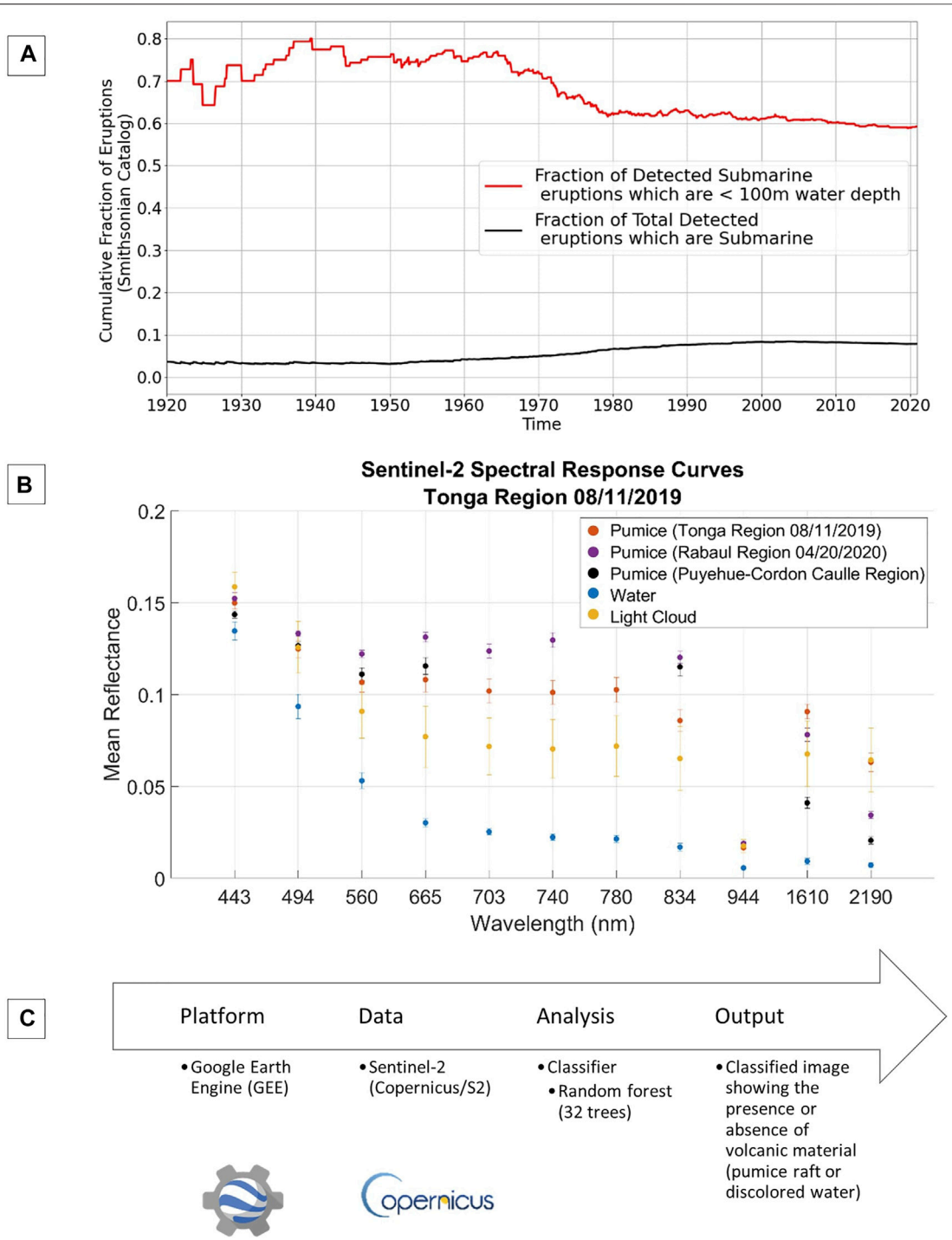

FIGURE 1 | (A) Fraction of all detected submarine eruptions out of total eruptions and fraction of detected shallow submarine eruptions (less than 100 m water depth) out of all detected submarine eruptions (Global Volcanism Program, 2013). Only a small fraction of submarine eruptions are pumice-forming. **(B)** Mean spectral response curves generated for a Sentinel-2 raft image in the Tonga region (11 August 2019). Error bars are generated from the standard deviation measured for each wavelength. Spectral response curves for pumice from the Rabaul region (20 April 2020) and a lake near Puyehue-Cordón Caulle are also provided for comparison. For Puyehue-Cordón Caulle, Sentinel-2 imagery was not available, so Landsat 8 imagery was used instead, and mean reflectance values were averaged between two dates (19 June 2013 and 5 October 2013). **(C)** Schematic of workflow used in this study.

and marine organisms across thousands of kilometers, potentially dispersing nutrients and increasing microbial biomass and biodiversity in areas geographically distant from the site of the eruption (DeVantier, 1992; Risso et al., 2002; Bryan et al., 2012). Pumice rafts can also be a significant hazard for human maritime activities, especially by clogging harbors and affecting near shore sea life and fisheries, disrupting local economies (Bryan et al., 2012; Jutzeler et al., 2020), as observed in the recent raft dispersal from the 2021 eruption of Fukutoku-Okanoba volcano, a submarine volcano in the Bonin Arc (24.285° N, 141.481° E) (Fauria et al., 2022; Yoshida et al., 2022).

Modern day submarine volcanism includes both mid-ocean ridge and ocean-island volcanism as well as fully/partially submarine subduction zone volcanism (e.g., Kermadec-Tonga Arc, Izu-Bonin Arc, Papua New Guinea Arc) (White et al., 2006; Global Volcanism Program, 2013). Overall, submarine volcanism potentially represents the majority (> 70%) of Earth's present-day volcanism (White et al., 2006; White et al., 2015; ERUPT, 2017; Rubin et al., 2012). However, we have historically detected only a very small fraction of expected underwater eruptions. In fact, only ~10% of all eruptions in the Smithsonian Global Volcanism database (Global Volcanism Program, 2013) over the past 100 years are submarine (**Figure 1A**, (White et al., 2006)) and the majority of detected eruptions are shallow (< 100 m water depth; **Figure 1A**).

One of the key reasons for this strong bias in our submarine eruption detection ability is the remote location of submarine volcanoes, as well as the difficulty in detecting eruptions that may or may not breach the sea surface. In addition, unlike subaerial volcanoes, precursory gas emissions or thermal anomalies are much more difficult to detect beneath the water surface. Although multiple new approaches have been proposed to improve submarine volcanism detection, including hydro-acoustics [e.g., (Heaney et al., 2013; Tepp et al., 2019)], seismic and ground deformation with ocean bottom seismometers (Wilcock et al., 2016; Matsumoto et al., 2019; Cesca et al., 2020; Tepp and Dziak, 2021), and ocean thermal anomalies (Baker et al., 1989; Mittal and Delbridge, 2019), challenges remain due to limited global instrumental coverage. In this study, we describe another dataset—satellite imagery—that can be used to efficiently detect and characterize products of submarine volcanism.

Automated satellite image analysis has already proven to be very useful for global subaerial eruption detections based on thermal anomalies, ash-rich subaerial plumes, and sulfur dioxide emissions (Wright et al., 2004; Brenot et al., 2014; Furtney et al., 2018; Poland et al., 2020; Engwell et al., 2021). However these methods are not adapted for submarine eruptions where the presence of water obscures/reduces these signatures. Satellite imagery has been used to map the eruptive products (e.g., pumice, ash, hydrothermal fluids) from submarine eruptions (Bryan et al., 2004; Jutzeler et al., 2014; O'Malley et al., 2014; Jutzeler et al., 2020; Sakuno, 2021; Whiteside et al., 2021) on an event-by-event basis. For example, a pumice raft from the 7 August 2019 Tonga eruption of an unnamed submarine volcano (sometimes referred to as Volcano F, 18.325°S, 174.365°W) in the Tofua Arc was tracked in near-real-time by Sentinel-2 (~10 m/pixel) and Landsat 8 (~30 m/pixel) satellite imagery (Jutzeler et al., 2020). However, this was done by manual hand-tracing and visual tracking through various satellite images. Although this process is fairly accurate for large rafts, it introduces subjectivity in tracing, especially for smaller rafts. Consequently, it is difficult to quantify uncertainties and biases across different studies. An ancillary challenge with using satellite imagery is the large data volume associated with satellite collections. For example, a single day in the Tonga region is composed of about forty individual 100 × 100 km image granules, each containing about 600 MB of data. Thus, analyzing entire global collections over extended time periods, and for multiple different satellites, would require handling enormous amounts of data and requisite computing resources.

Our study aims to address these challenges of submarine eruption detection by developing a semi-automated Machine-Learning (ML) based methodology using global, publicly available, high resolution (~ <30 m/pixel) satellite data products (**Figure 1C**). This method utilizes Google Earth Engine (Gorelick et al., 2017), in order to remove the large data storage need that is typical for analyzing satellite collections. Our primary focus is on detecting rafts formed from floating pumice (or pumiceous material, **Supplementary Text S16**) emitted by intermediate to silicic volcanism, but our approach can be applied to other signatures of submarine eruptions (e.g., discolored water from hydrothermal fluids). Our analysis is complementary to recent work on detection of large submarine eruptions using specific global, low resolution (> 250 m/pixel) satellite products (O'Malley et al., 2014; Qi et al., 2020; Whiteside et al., 2021).

As a complementary question, we also seek to examine whether individual pumice raft detections necessarily indicate a new eruption. Previous work has examined the remobilization of pumice clasts, which may have been deposited in the area immediately surrounding the vent, or stranded a distance away after traveling as a raft, following large eruptions (Mandeville et al., 1996; Shane et al., 1998; Manville et al., 2002; Jutzeler et al., 2020). Using our automated detection algorithms, we can improve raft detection (of scales of at least a few pixel scale, e.g., a few 100 m^2 for Sentinel-2 imagery and even smaller with commercial sub-m pixel scale imagery). These observational constraints on pumice raft occurrence, along with field studies of the detected rafts and textural analysis, can help understand the re-rafting mobility and floatation ability of pumice of different sizes on timescales ranging from days to hundreds of years after the original eruption (Brasier et al., 2011; Bryan et al., 2012).

In **Section 2**, we describe our detection algorithm and its implementation in Google Earth Engine. In **Section 3**, we illustrate our method's accuracy using satellite imagery from the 2019 Tonga submarine eruption (Jutzeler et al., 2020) and then use our method to analyze pumice rafts in a region close to the Rabaul volcano in Papua New Guinea (partially submerged caldera). In **Section 4**, we discuss what our new pumice raft detections from Rabaul suggest in regards to suspension of pumice material, potentially from pumice clasts or rafts previously washed up on shores or eroded on riverbanks or coastal cliffs. Finally, we briefly discuss areas for future algorithmic improvements.

2 MATERIALS AND METHODS

2.1 Google Earth Engine

We developed and implemented our Machine Learning (ML) detection algorithm for pumice raft detection on the Google Earth Engine (GEE) platform (Gorelick et al., 2017). GEE is a web-based, publicly available platform that enables access to a vast catalog of satellite images and the resources to run global-scale analyses without the need to download or export large amounts of data. There are various satellite collections offered through GEE, such as low resolution (MODIS) and medium-high resolution imagery (Landsat, Sentinel-2). Although some other super-high-resolution image collections are available outside of GEE (e.g., Planet labs—3 m/pixel, Digital Globe—50 cm/pixel), they are typically not publicly available without commercial licenses. Thus, for this study, we have primarily focused on using GEE resources for the ML algorithm.

Specifically, we use GEE collections from the Sentinel-2 Multi-Spectral Instrument (MSI) as our baseline satellite product. Sentinel-2 (a pair of two satellites, each with MSI instrumentation) offers both high-resolution imagery (10–60 m/pixel), good coverage in regions of interest, and a relatively frequent repeat time (~global 5-day revisits; **Supplementary Text S6**). Sentinel-2 data products are also freely available through the European Space Agency's Copernicus Open Access Hub as well as other cloud environments. For our study, we chose to use Sentinel-2 as its high resolution imagery could be used to detect much smaller rafts than a lower resolution satellite (e.g., MODIS). In addition, Sentinel-2's MSI collects data across 13 different spectral bands, with finer spectral coverage than other high resolution satellite image collections (e.g., Landsat 7 and 8) (See spectral response curve for Landsat 8 image of Puyehue-Cordón Caulle pumice in **Figure 1B**). An initial method using thresholds on only the visual bands to detect pumice rafts was insufficient, so the additional spectral bands are necessary in our ML algorithm (**Supplementary Text S1**). As illustrated by the variable importance in the Random Forest classifier (RF, **Supplementary Figure S11**), the multi-wavelength information is critical for accurate classification with a dominant role of the visible bands. In particular, the reflectance of pumice in the near-infrared (NIR) bands (700–900 nm) is much higher than the reflectance at those bands of most biological phenomena that are near the surface but still underwater (i.e., algal blooms, coral spawn, seaweed) (Biermann et al., 2020; Qi et al., 2020), so the NIR bands are critical for distinguishing between pumice and other visually similar-looking biological blooms. Our overall methodology is general and can be applied to other satellite collections in the future (**Supplementary Text S10**).

2.2 Machine-Learning Algorithm

To identify spectral characteristics that can be used to classify Sentinel-2 image pixels as pumice rafts, we generated spectral response curves for pumice and other categories of interest in **Figure 1B**. Spectral response curves record the mean reflectance or brightness of an image pixel for a range of wavelengths. We used the Tonga pumice raft from 11 August 2019 to generate the spectral response curves (**Figure 1B**), as the particular eruption and the associated raft has been extensively analyzed by previous work (Brandl et al., 2020; Jutzeler et al., 2020). We also show the variance around the mean spectral response curve calculated for all of the pixels for each class (pumice, water, light clouds).

A key result from this analysis is that there is a significant difference between the spectral response curves of pumice, water, and light clouds (**Figure 1B**). Additionally, we find relatively minor (compared to differences with other classes) variation in the reflectance from pumice pixels within a single geo-temporal area, such as a specific day in Tonga (**Figure 1B**) or comparing across multiple days for the same raft (**Supplementary Figure S16**). Although there is some variation in pumice spectral response curves when comparing rafts from different chemical compositions, sources, and times (**Figure 1B**, comparison with Rabaul raft and Puyehue-Cordón Caulle raft), the general shape of the reflectance curve remains very similar. This characteristic shape of the spectral response curve for pumice pixels allows for an algorithm to identify pumice and differentiate from other classes (e.g., water, clouds) across a broad range of regions and time periods. Details for the Puyehue-Cordón Caulle raft are provided in **Supplementary Text S13**.

Our machine-learning algorithm uses a Random Forest classifier to read in an RGB Sentinel-2 image and return a classified image, where each pixel is colored according to the assigned class. The algorithm specifics are detailed in **Supplementary Text S4**. Since RF is a supervised learning algorithm, we need to train it on a set of manually demarcated and classified pixels. Our primary training data for pumice, ocean water, light cloud cover, and heavy cloud cover was sampled from the Tonga raft on 11 August 2019 (**Figure 2A**, only a small part of the raft pixels were used for training). We also included additional data from a Sentinel-2 scene of Rabaul, Papua New Guinea, on 20 April 2020 (**Figure 2B**, spectrally this is representative of the potential rafts from other days also). This image includes a large, distinct pumice raft as well as ocean water, light cloud cover, pumice mixture classes, and two different discolored water classes (additional information for the discolored water classes are included in **Supplementary Text S9**). Since the discolored water classes are not the primary focus of this study, our primary optimization for the RF algorithm was to ensure accurate detection of pumice rafts. We provide all the scripts, with step-by-step instructions for usage, used in our analysis in a publicly available repository (**Supplementary Material**—GEE Script Links).

3 RESULTS

3.1 Single Image Analysis Results

We applied our classification algorithm to Sentinel-2 images from different geo-temporal regions to test model accuracy (**Figure 2**). In the Tonga area on 11 August 2019 (**Figure 2A**), the classifier displays pumice pixels in red, water in blue, light cloud cover in orange, and heavy cloud cover in white. The shape of the large raft is distinctly visible in the classified image. In the Rabaul region, on

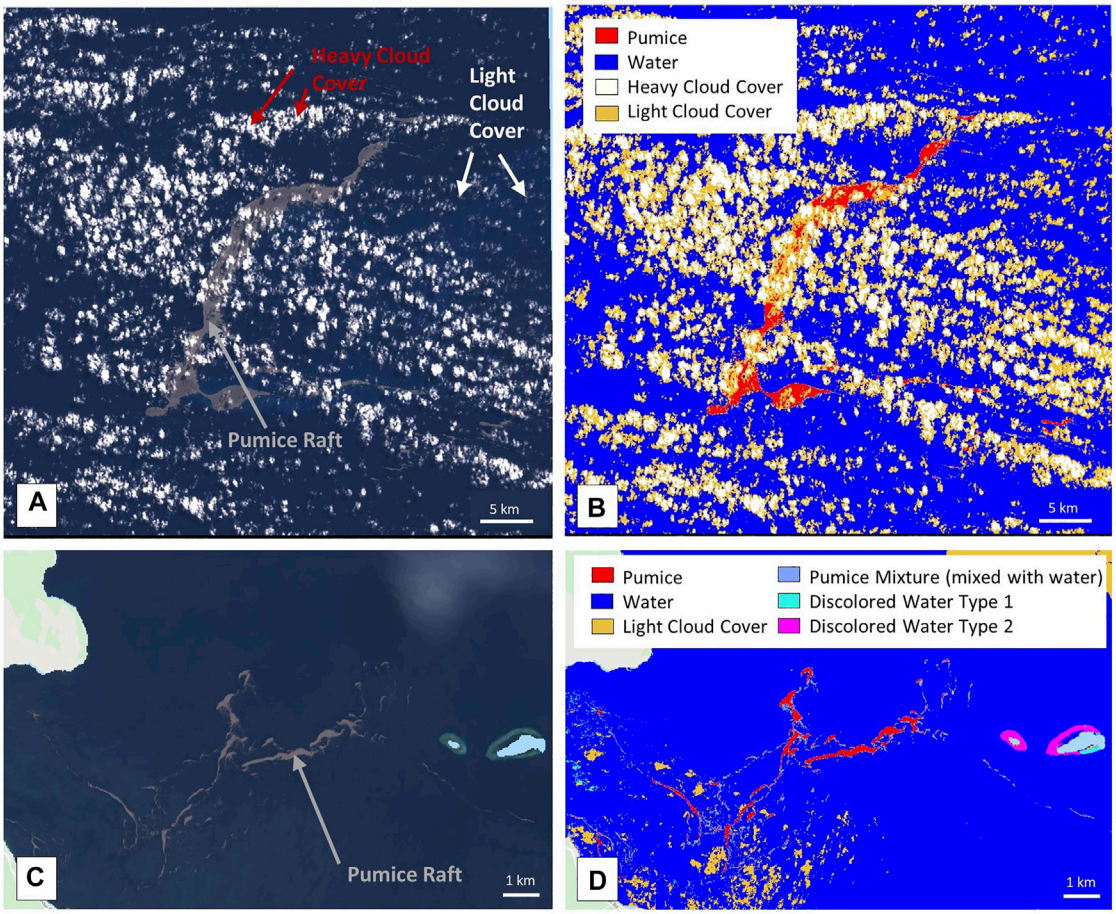

FIGURE 2 | (A) Land-masked RGB image of Tonga region on 08/11/2019 **(B)** Classified image of Tonga region on 08/11/2019 **(C)** Land-masked RGB image of Rabaul on 04/20/2020 **(D)** Land-masked classified image of Rabaul on 04/20/2020.

20 April 2020 (**Figure 2A**), the classifier also includes additional classes: mixed/faint pumice—a mixture of water and pumice—shown in light blue, and two different classes of discolored water shown in turquoise and magenta. Overall, our algorithm is efficient at identifying pumice from other backgrounds though the accuracy of discolored water detection (mixing with corals) and shallow cloud is not great at present. Algorithm validation methods and results are included in **Supplementary Text S5**.

3.2 Regional Results

To assess the utility of our algorithm for new submarine eruption detection, we applied the classifier over a single region for an extended period of time. We focused on Rabaul, a partially submarine volcano located on the Gazelle Peninsula's tip at the northeast end of New Britain in Papua New Guinea (**Figure 3A**). The Rabaul caldera (~8 × 14 km size) was formed as a consequence of multiple large explosive eruptions in the past few hundred thousand years, with the present day shape due to an eruption ~1,400 years ago (GVP and wunderman, 1994). The caldera is mostly shallow submarine (< 200 m water depth) and is connected to the sea on the east through a wide opening (Blanche Bay). The main raft-forming eruptions for this volcano occurred in 1878, 1937, and 1994, and no raft formation has been recorded since 1994 (GVP and Wunderman, 1994; GVP and Wunderman, 2006). No activity has been recorded at either of the main vents (Vulcan and Tavurvur) since 2014 (Bernard and Bouvet de Maisonneuve, 2020). More detailed eruption history is provided in **Supplementary Text S8**.

In the Rabaul area, we applied our algorithm from November 2015 (start of the Sentinel-2 coverage for the Rabaul region) to August 2020—a total of 239 distinct days with images. More details on our algorithm application method are included in **Supplementary Text S7**.

Of these 239 days, we found that 74 days were too cloudy for the classifier to detect any pumice meaningfully. Cloudy days were filtered out by manually examining classified images and removing images in which every pixel was labeled as heavy or light cloud cover. In the future, this step can be automated by explicitly filtering the images based on the classified heavy cloud fraction. We detected potential rafts in 28 (red lines, **Figure 3B**)

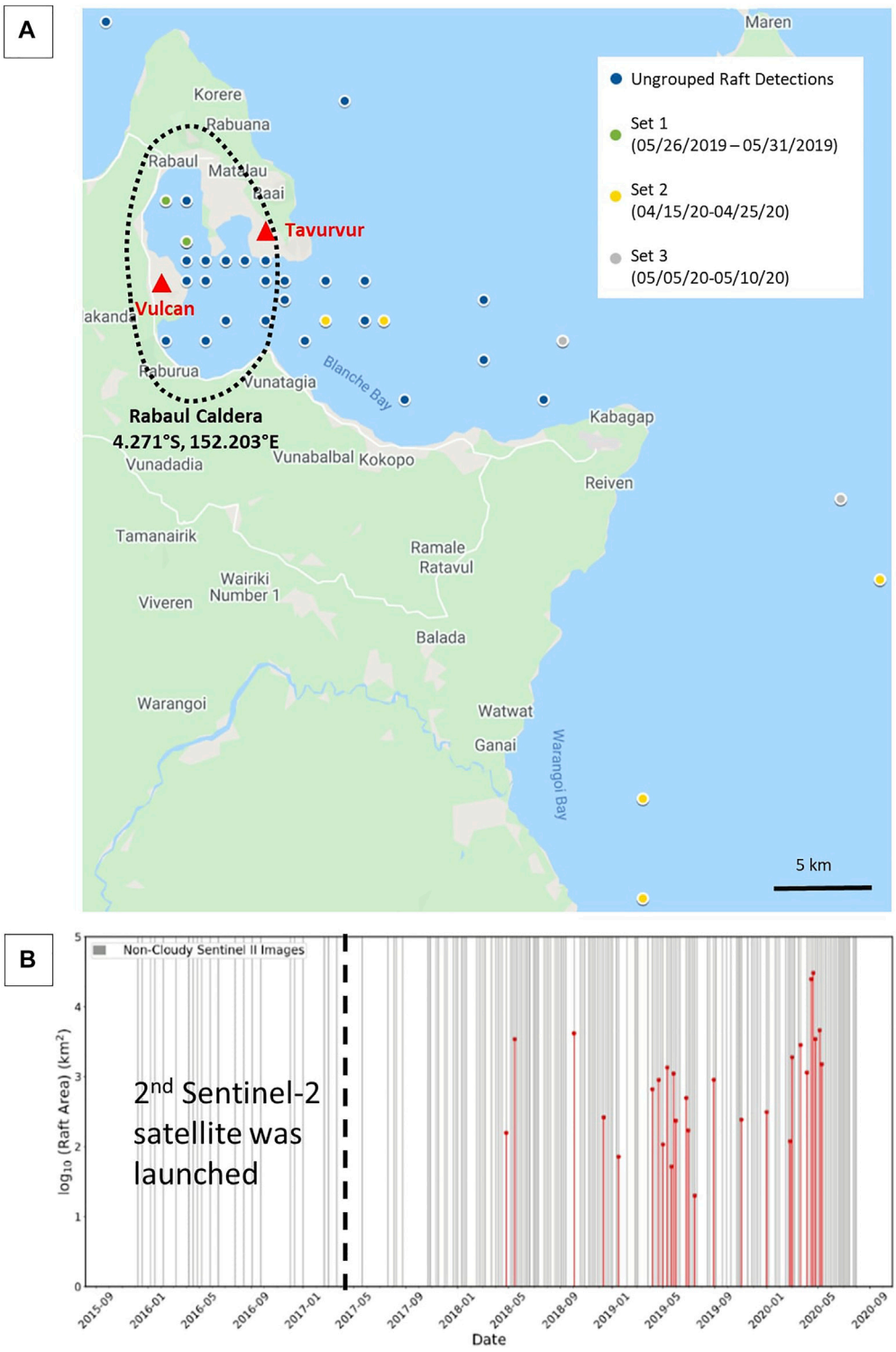

FIGURE 3 | (A) Map of pumice raft detection locations in Rabaul area. Main vent locations are marked with red triangles. Groupings of raft detections (by proximity in time and location) are indicated by the different colored icons **(B)** Non-cloudy days during Sentinel-2 coverage period, with raft detections in red (height indicating raft area).

of the remaining 165 days (gray lines, **Figure 3B**), leading to a detection rate of 16.97%. As illustrated in **Figure 3B**, most of our raft detections were after January 2018 (**Figure 3B**). This is likely a consequence of increased revisit frequency (~5-day) after the second Sentinel-2 satellite launch. Before 2018, when only one Sentinel-2 satellite was in operation, there are significantly fewer images available. It is noteworthy that none of the rafts detected in our analysis had been previously reported in the scientific literature (to the best of our knowledge) or the Smithsonian Global Volcanism Catalog (Global Volcanism Program, 2013). The sizes of our detected rafts varied greatly, with raft areas as small as 20 km^2 to as great as 10,000 km^2. At present, we do not have any direct ground truthing of our detections. However, considering the distinctive spectral features of pumice compared to other biological sources, especially in the Near Infrared (Biermann et al., 2020; Qi et al., 2020), we interpret the classified features as rafts of pumiceous material - pumice rafts (**Supplementary Text S16** for discussion regarding difference between "true" pumice and more general pumiceous material).

3.2.1 Source of New Rafts in Rabaul

Given our new raft detections, there is a natural follow-up question—do these rafts represent previously unreported submarine eruptions, or are they suspended pumiceous material remobilized from known previous eruption deposits from Rabaul or pumice produced by eruptions from other volcanoes in the region that subsequently drifted into the Rabaul harbor? These are the three primary end-member models, with the remobilization of pumice (or pumiceous material) from previous eruptions being a process that has been documented following the dispersal of large pumice rafts. For example, the Tonga 2019 pumice raft was stranded in near coastal regions in multiple islands in Fiji (in particular Lakeba island) in early-mid September 2019. However, some of this raft material in Lakeba island was not remobilized till late October-early November 2019 (Jutzeler et al., 2020, observations from Sentinel-2 Imagery). Redeposition and remobilization of volcanic products such as ash fall (Etyemezian et al., 2019; Del Bello et al., 2021) as well as subaerial [e.g., from Pinatubo 1991 eruption, Torres et al. (1996)] and subaqueous pyroclastic material has been recorded after initial deposition (Mandeville et al., 1996; Manville et al., 2002; Park and Schmincke, 2020). However, the majority of this work has focused on a short time frame—on the order of days to months after the eruption though there are some exceptions—e.g., secondary pumice rafts from Socorro Island in January 2009 (Ochoa, 2009, Personal Comm. from Scott Bryan) and secondary pumice rafts in Brasier et al. (2011). Here, if our hypothesis is correct, the pumiceous material we are seeing is remobilized tens or even hundreds of years after the original eruption since the last major raft forming eruption in Rabaul was in 1994.

We assess the likelihood of new submarine eruptions by analyzing the reported volcanic activity for Rabaul in the Smithsonian Volcano Catalog (Global Volcanism Program, 2013). The Rabaul Volcano Observatory has recorded no large eruptions since 2014 (Global Volcanism Program, 2013) and/or any significant submarine activity besides hydrothermal discharge near the Tavurvur vent. Because rafts initiating from point sources can indicate new eruptions, we test this further by recording each of our raft detections' spatial location and considering the spread of each sighting. We have tried to manually aggregate three sets of raft locations together (**Figure 3A**). These sets are of sequential images, in which the raft detections were somewhat close, not only in time, but in location as well. Conclusively tracking the rafts as they are advected around by local ocean currents is challenging due to repeat frequency (5-day gap between images), cloud cover, and complex shallow-water ocean currents in the regions. In aggregate, the detections are scattered over a broad area in the caldera and surrounding sea, rather than primarily located near any known vents (**Figure 3A**).

We also used Sentinel-2 imagery as well as ancillary datasets [e.g., higher spatial and temporal resolution Planet Labs imagery (Planet Team, 2021)] to check if the rafts are associated with any other eruptive signatures expected for shallow submarine eruptions (e.g., aerial plumes, discolored water). We did not find any aerial plumes and, while there was some discolored water around the Tavurvur vent location, we did not find any relationship between the days with raft detections and days with discolored water around the vent (**Supplementary Text S14**). Thus, we interpret that the detected rafts are not actually products from a new submarine eruption.

Instead, we propose that they are secondary rafts [like the rafts in Socorro Island in January 2009 (Ochoa (2009), Personal Comm. from Scott Bryan); also see Richards (1958), Lee (1979), Kent and Frick (1984), Thiel and Gutow (2004) for related discussion] that have been suspended after being deposited on surrounding shores and riverbanks following their initial eruptions tens to hundreds of years ago (**Section 4** for the potential processes). This is a new, novel physical process that has not been fully documented before, especially in the modern/satellite era. Our analysis is the first study, to the best of our knowledge, to carefully document the secondary raft process on timescales of years or longer using satellite imagery, further validating the importance of this process as suggested by previous studies (Pullar et al., 1977; Osborne et al., 1991; Shane et al., 1998; Bryan et al., 2012; Jutzeler et al., 2014). This secondary raft process is likely relevant for the dispersal of eruptive products from many volcanic systems in coastal regions (e.g., Krakatau in Indonesia, Tonga-Fiji region). Although the secondary rafts are much smaller scale individually compared to large pumice rafts associated with new eruptions such as the Havre 2012 and the Krakatau 1883 eruption, they can be much more frequent. Thus, they may potentially still be important for material transport and local/regional scale biology. We acknowledge that a systematic analysis of secondary rafts on regional/global scales is needed to quantify this effect (if any). Without any specimens of the pumice that we detected, we are presently unable to ascertain a specific source eruption of the rafts. In addition, even with samples, it may still be difficult to determine the original source eruption or eruptions, as pumice material from the 1878 eruption and subsequent eruptions have very similar overall composition and texture (Bernard and Bouvet de Maisonneuve, 2020). However, the morphology of the pumice samples (angular vs. rounded, presence of biological material) can at least provide some constraints on whether the pumice represents a new eruption or remobilized material (from Rabaul or other farther eruptions, based on composition).

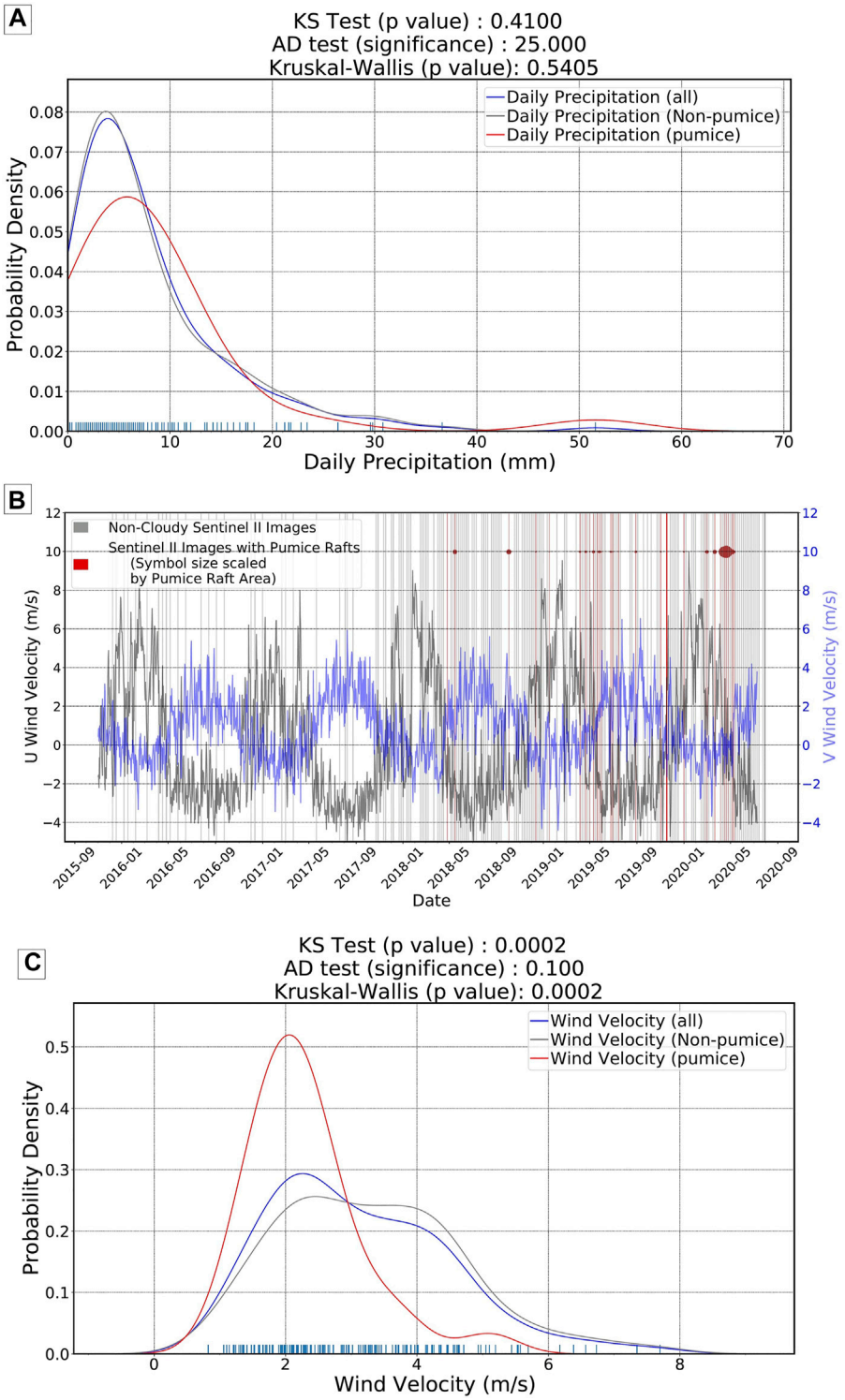

FIGURE 4 | (A) Probability density function for the daily precipitation in the Rabaul region (5 days rolling window) **(B)** Time series of daily wind directionality in the Rabaul region—U wind velocity is the eastward component of wind while the V wind velocity is the northward component **(C)** Probability density function for daily wind magnitude in the Rabaul region (5 days rolling window).

Furthermore, field work in the Rabaul region can ground truth our conclusions and help test whether there is enough erodible material in the coastal areas to form rafts.

4 DISCUSSION

4.1 Source of Pumice Remobilization: Influence of Weather Factors

Considering our interpretation that the detected rafts in Rabaul are secondary rafts, an important question to consider is what potential physical mechanisms are responsible for the mobilization of pumiceous material. One possibility is that resuspension is a consequence of local climatological conditions, e.g., high rainfall events, high wind conditions that dislodge pumice along coastlines and riverbanks back into the water. Local weather can lead to landslides and dislodgement of small pumice rafts [e.g., local pumice raft from rockslide in the Askja caldera, Iceland on 21 July 2014 (Icelandic Meteorological, 2014)]. Using ERA5 Daily Aggregate Reanalysis Product (Hersbach et al., 2020) (directly accessible through GEE), we generated time series of various atmospheric properties—daily mean air temperature, wind magnitude, wind direction, and precipitation. These time series were all sampled from the same location, directly on top of one of Rabaul's vents, and the time series spanned the entire Sentinel-2 coverage period in the area. We did not observe any significant correlation between the daily mean air temperature and the detection of pumice rafts in the area (**Supplementary Figure S3**). We also explored potential correlations with weather parameters up to 10 days before raft detection to allow for some unknown advection time (**Supplementary Data**). Overall, we did not find significantly different results across these windows. The main statistically robust relationships in our dataset are between raft detection and wind and precipitation.

4.1.1 Precipitation

To compare the impact of wind, precipitation, and other weather parameters on raft detection, we construct and compare probability density distributions (PDF). A PDF is a function that provides the relative likelihood of an event (raft detection) given another parameter (e.g. wind speed, recorded rainfall). We find that the PDF for the days with sighted pumice rafts (red curve, **Figure 4A**) were slightly different from the curves for the total days in the coverage period (blue curve, **Figure 4A**) and the days where no rafts were detected (gray curve, **Figure 4A**) (using 5 day rolling window, other windows have similar results). However, this difference is not statistically significant when using either the Anderson-Darling (AD) test statistic (Scholz and Stephens, 1987) or the Epps-Singleton (ES) test statistic (Epps and Singleton, 1986). The medians of the raft vs. non-raft precipitation PDFs are potentially different, as shown by the lower p-value for the Kruskal-Wallis test (Kruskal and Wallis, 1952). We also do not find any clear correlation between precipitation values and raft area.

We analyzed the long-term precipitation history in the Rabaul area to help elucidate the remobilization process. We used ERA5 data to consider 3-day rolling sums of precipitation values in Rabaul since 1990. From the long-term history, we observe the peak precipitation occurred in February 2018. All of our detected rafts in Sentinel-2 imagery are post 2018 (further analysis using Landsat imagery is included in **Supplementary Text S15**). This may be a consequence of increased frequency of sampling in the Rabaul area after the second Sentinel-2 satellite launch in March of 2017. Alternatively, the detection of rafts after the precipitation peak in early 2018 suggests that a large storm or significant weather event made rafts easier to remobilize post-2017. More detailed work, especially in the field in Rabaul, is needed to test these hypothesis and ascertain which coastal areas have significant amounts of pumice ready to mobilize.

Overall, we find that there is only a weak correlation between precipitation and raft detection. We posit that the slightly higher values for precipitation before raft detection compared to non-raft days suggest a role for higher precipitation to increase erosion and consequently encourage raft remobilization. However, it is clear that precipitation is not a unique factor since days of high precipitation are not always followed by raft detections (**Figure 4A**, **Supplementary Figure S2**).

4.1.2 Wind

In addition to precipitation, we also considered the role of wind in raft formation. **Figure 4B** shows the daily wind direction [U (eastward), V (northward) components] in Rabaul along with red vertical lines highlighting days with raft detections. We find that the general wind direction in Rabaul has a strong seasonal cycle which is relatively stable over the past 5 years. Interestingly, most of our pumice raft sightings were around the March–May window despite having a number of non-cloudy images for other months. This suggests that there is some seasonality to the raft remobilization process.

In order to assess the role of overall wind magnitude, we show the probability distribution curves for wind velocity for all days in the Sentinel-2 coverage period (blue curve, **Figure 4C**), days without raft sightings (gray curve, **Figure 4C**), and days with raft sightings (red curve, **Figure 4C**) (using 5 day rolling window, other windows have similar results). We find that days where rafts were detected produced a significantly different probability distribution curve (**Figure 4C**). There is also a high correlation between wind amplitude and raft area (**Supplementary Figure S3**). However, since there are not many high raft area data points, the correlation may be biased by outliers. Overall, we see most of our raft sightings are in the distinct range of wind velocities (1 to 4 m/s) compared to the overall distribution. Even when accounting for different sample sizes, this difference is statically significant [Anderson-Darling (AD) test statistic (Scholz and Stephens, 1987); the Epps-Singleton (ES) test statistic (Epps and Singleton, 1986); Kolmogorov-Smirnov (KS) test (Hodges, 1958)]. We conclude that the high wind velocities likely break up and disperse the secondary rafts too rapidly for Sentinel-2 to capture. We would note that there are number of non-cloudy days with low wind velocity and no raft detection (**Figure 4C**, grey curve). Thus, wind condition is not the only parameter that controls the temporal pattern of raft detection with an additional role of seasonality.

4.2 Open Challenges for Global Pumice Detection Algorithm

Although our ML algorithm is reasonably successful for pumice raft detection, it is not fully automated. The classification process requires manual checks to filter out incorrect classifications of pumice and cloud cover. In particular, the light cloud cover with a flat spectral response curve can at times be misclassified as pumice (and vice versa). Also, the satellite's viewing geometry may create a "Sun glint" in certain images, where all of the pixels in the RGB rendering are affected and off-colored. The classifier subsequently has difficulty correctly identifying the correct class of each pixel. There are some ways these issues can be addressed. Better atmospheric corrected products, specifically for oceanic regions, would help improve detection. For instance, in some cases, using the atmosphere corrected Surface Reflectance (Level-2A) product can allow us to detect pumice rafts on images discolored due to atmospheric effects (**Supplementary Figure S10**). Alternatively, more stringent data filtering for satellite viewing angle and cloudiness bounds can help reduce potential false positives. Finally, incorporating additional satellite imagery data e.g., geostationary imagery with high temporal frequency (more detailed raft tracking as well as better cloud detection based on motion) and radar imagery (sensitive to surface roughness and reduced sensitivity to atmospheric effects) could help improve detection accuracy. Additional potential options for algorithmic improvement are described in **Supplementary Text S11**.

5 CONCLUSION

In this study, we show that GEE and RF classifiers can be successfully used to detect pumice rafts. This can be useful to efficiently track pumice rafts, which can pose as hazards and disruptions to boats and harbors (Jutzeler et al., 2014; Jutzeler et al., 2020) and thus help with hazard mitigation and coordination services along populated shorelines (e.g., ongoing raft arrival on mainland Japan from the August 2021 eruption of Fukutoku-Okanoba volcano). Our methodology can help address our current strong bias in eruption detection and improve the detection of submarine eruptions globally. Using GEE removes the large data storage requirement and allows for a semi-automated, easily scalable classification with minimal subjective biases. Using the Rabaul caldera regions in Papua New Guinea as a case study, we show that not all detected pumice rafts necessarily correlate with a new eruption. Indeed, in some coastal regions, remobilization is likely to be a widespread phenomenon and can affect the spatial pattern of how products from an eruption are deposited as well as pumice remobilization after large storms/coastal tsunamis (e.g., Anak Krakatau 2018; Hunga Tonga Hunga Ha'apai 2022 eruption). Since these spatial patterns serve as the basis for estimating volcanic eruptive volumes, as well as long-distance (on tens to hundreds of kilometers scale) stratigraphic correlations (Shane et al., 1998; Mouginis-Mark and Zimbelman, 2020; Freundt et al., 2021), the raft remobilization process needs to be further analyzed. Finally, if drifting, remobilized pumice is common, its presence can impact the detection of future submarine eruptions, especially small eruptions in near coastal regions. Thus understanding the morphology, abrasion, and lifetime of the remobilized rafts (i.e., how they fragment over time and any differences from newly erupted rafts) is critical to remove this false positive for new eruption detection.

DATA AVAILABILITY STATEMENT

The original contributions presented in the study are publicly available. This data can be found here: https://figshare.com/projects/Pumice_Raft_Detection_Using_Machine-Learning_on_Multispectral_Satellite_Imagery/126466.

AUTHOR CONTRIBUTIONS

TM and MZ conceived the study and were in charge of overall direction and planning. MZ wrote the algorithm scripts and applied algorithm in case study. TM and MZ analysed the data and wrote the manuscript with input from all authors.

ACKNOWLEDGMENTS

We thank Amber Madden-Nadeau, Samantha L. Engwell, Sebastian Watt, Michael Cassidy, Ralf Bennartz, Ashok Gupta, Liam Kelly, John Rausch for useful discussions and suggestions for the manuscript text. We thank the editor and the reviewers for their valuable comments and suggestions. We thank Planet Labs, Sentinel-2, Landsat 7/8, and Google Earth Engine platform for providing the satellite imagery and computational tools. MZ acknowledges support from the MIT UROP program, TM acknowledges funding support from the Crosby Postdoc Fellowship at MIT, and KF acknowledges funding support from the NASA Grant 80NSSC20K1450.

SUPPLEMENTARY MATERIAL

The Supplementary Material for this article can be found online at: https://www.frontiersin.org/articles/10.3389/feart.2022.838532/full#supplementary-material

REFERENCES

Baker, E. T., Lavelle, J. W., Feely, R. A., Massoth, G. J., Walker, S. L., and Lupton, J. E. (1989). Episodic Venting of Hydrothermal Fluids From the Juan de Fuca Ridge. *J. Geophys. Res.* 94, 9237–9250. doi:10.1029/jb094ib07p09237

Bernard, O., and Bouvet de Maisonneuve, C. (2020). Controls on Eruption Style at Rabaul, Papua New Guinea - Insights from Microlites, Porosity and Permeability Measurements. *J. Volcanology Geothermal Res.* 406, 107068. doi:10.1016/j.jvolgeores.2020.107068

Biermann, L., Clewley, D., Martinez-Vicente, V., and Topouzelis, K. (2020). Finding Plastic Patches in Coastal Waters Using Optical Satellite Data. *Sci. Rep.* 10, 5364. doi:10.1038/s41598-020-62298-z

Brandl, P. A., Schmid, F., Augustin, N., Grevemeyer, I., Arculus, R. J., Devey, C. W., et al. (2020). The 6-8 Aug 2019 Eruption of 'Volcano F' in the Tofua Arc, Tonga. *J. Volcanology Geothermal Res.* 390, 106695. doi:10.1016/j.jvolgeores.2019.106695

Brasier, M. D., Matthewman, R., McMahon, S., and Wacey, D. (2011). Pumice as a Remarkable Substrate for the Origin of Life. *Astrobiology* 11, 725–735. doi:10.1089/ast.2010.0546

Brenot, H., Theys, N., Clarisse, L., van Geffen, J., van Gent, J., Van Roozendael, M., et al. (2014). Support to Aviation Control Service (SACS): an Online Service for Near-Real-Time Satellite Monitoring of Volcanic Plumes. *Nat. Hazards Earth Syst. Sci.* 14, 1099–1123. doi:10.5194/nhess-14-1099-2014

Bryan, S. E., Cook, A., Evans, J. P., Colls, P. W., Wells, M. G., Lawrence, M. G., et al. (2004). Pumice Rafting and Faunal Dispersion during 2001-2002 in the Southwest Pacific: Record of a Dacitic Submarine Explosive Eruption from Tonga. *Earth Planet. Sci. Lett.* 227, 135–154. doi:10.1016/j.epsl.2004.08.009

Bryan, S. E., Cook, A. G., Evans, J. P., Hebden, K., Hurrey, L., Colls, P., et al. (2012). Rapid, Long-Distance Dispersal by Pumice Rafting. *PloS one* 7, e40583. doi:10.1371/journal.pone.0040583

Cesca, S., Letort, J., Razafindrakoto, H. N. T., Heimann, S., Rivalta, E., Isken, M. P., et al. (2020). Drainage of a Deep Magma Reservoir Near Mayotte Inferred from Seismicity and Deformation. *Nat. Geosci.* 13, 87–93. doi:10.1038/s41561-019-0505-5

Del Bello, E., Taddeucci, J., Merrison, J. P., Rasmussen, K. R., Andronico, D., Ricci, T., et al. (2021). Field-Based Measurements of Volcanic Ash Resuspension by Wind. *Earth Planet. Sci. Lett.* 554, 116684. doi:10.1016/j.epsl.2020.116684

DeVantier, L. (1992). Rafting of Tropical Marine Organisms on Buoyant Corolla. *Mar. Ecol. Prog. Ser.* 86, 301–302. doi:10.3354/meps086301

Embley, R. W., Baker, E. T., Chadwick, W. W., Lupton, J. E., Resing, J. A., Massoth, G. J., et al. (2004). Explorations of Mariana Arc Volcanoes Reveal New Hydrothermal Systems. *Eos Trans. AGU* 85, 37–40. doi:10.1029/2004eo040001

Engwell, S., Mastin, L., Tupper, A., Kibler, J., Acethorp, P., Lord, G., et al. (2021). Near-real-time Volcanic Cloud Monitoring: Insights into Global Explosive Volcanic Eruptive Activity through Analysis of Volcanic Ash Advisories. *Bull. Volcanology* 83, 1–17. doi:10.1007/s00445-020-01419-y

Epps, T. W., and Singleton, K. J. (1986). An Omnibus Test for the Two-Sample Problem Using the Empirical Characteristic Function. *J. Stat. Comput. Simulation* 26, 177–203. doi:10.1080/00949658608810963

Erupt (2017). *Volcanic Eruptions and Their Repose, Unrest, Precursors, and Timing*. Washington, DC: The National Academies Press. doi:10.17226/24650

Etyemezian, V., Gillies, J. A., Mastin, L. G., Crawford, A., Hasson, R., Van Eaton, A. R., et al. (2019). Laboratory Experiments of Volcanic Ash Resuspension by Wind. *J. Geophys. Res. Atmos.* 124, 9534–9560. doi:10.1029/2018jd030076

Fauria, K., Jutzeler, M., Mittal, T., Gupta, A., Kelly, L., Rausch, J., et al. (2022). Simultaneous Creation of a Large Vapor Plume and Pumice Raft by a Shallow Submarine Eruption. *Earth Space Sci. Open Archive*. doi:10.1002/essoar.10510412.1

Freundt, A., Schindlbeck-Belo, J. C., Kutterolf, S., and Hopkins, J. L. (2021). *Tephra Layers in the Marine Environment: A Review of Properties and Emplacement Processes*. London: Geological Society. *Special Publications* 520.

Furtney, M. A., Pritchard, M. E., Biggs, J., Carn, S. A., Ebmeier, S. K., Jay, J. A., et al. (2018). Synthesizing Multi-Sensor, Multi-Satellite, Multi-Decadal Datasets for Global Volcano Monitoring. *J. Volcanology Geothermal Res.* 365, 38–56. doi:10.1016/j.jvolgeores.2018.10.002

Gorelick, N., Hancher, M., Dixon, M., Ilyushchenko, S., Thau, D., and Moore, R. (2017). Google Earth Engine: Planetary-Scale Geospatial Analysis for Everyone. *Remote sensing Environ.* 202, 18–27. doi:10.1016/j.rse.2017.06.031

Global Volcanism Program (2013). "Global Volcanism Program," in *Volcanoes of the World*. Editor E. Venzke (Smithsonian Institution), 2, 4–6. doi:10.5479/si.GVP.VOTW4-2013

Gvp (1994). "Report on Rabaul (Papua New Guinea)," in *Bulletin of the Global Volcanism Network*. Editor R. Wunderman (Smithsonian Institution), 19, 8. doi:10.5479/si.GVP.BGVN199408-252140

Gvp (2006). "Report on Rabaul (Papua New Guinea),". Editor R. Wunderman (Smithsonian Institution), 31, 9. doi:10.5479/si.GVP.BGVN200609-252140*Bull. Glob. volcanism Netw.*

Heaney, K. D., Campbell, R. L., and Snellen, M. (2013). Long Range Acoustic Measurements of an Undersea Volcano. *The J. Acoust. Soc. America* 134, 3299–3306. doi:10.1121/1.4818844

Hersbach, H., Bell, B., Berrisford, P., Hirahara, S., Horányi, A., Muñoz-Sabater, J., et al. (2020). The ERA5 Global Reanalysis. *Q.J.R. Meteorol. Soc.* 146, 1999–2049. doi:10.1002/qj.3803

Hodges, J. L. (1958). The Significance Probability of the Smirnov Two-Sample Test. *Ark. Mat.* 3, 469–486. doi:10.1007/bf02589501

Icelandic Meteorological Office (2014). *Rockslide in Askja, July 21 2014 - Preliminary Results of Observations*.

Jutzeler, M., Marsh, R., Carey, R. J., White, J. D., Talling, P. J., and Karlstrom, L. (2014). On the Fate of Pumice Rafts Formed during the 2012 Havre Submarine Eruption. *Nat. Commun.* 5, 3660. doi:10.1038/ncomms4660

Jutzeler, M., Marsh, R., van Sebille, E., Mittal, T., Carey, R. J., Fauria, K. E., et al. (2020). Ongoing Dispersal of the 7 August 2019 Pumice Raft from the Tonga Arc in the Southwestern Pacific Ocean. *Geophys. Res. Lett.* 47, e1701121. doi:10.1029/2019gl086768

Kelley, D. (2017). Volcanology: Vulcan Rule beneath the Sea. *Nat. Geosci.* 10, 251–253. doi:10.1038/ngeo2929

Kent, L., and Frick, C. (1984). Drift Pumice in the Indian and South Atlantic Oceans. *South. Afr. J. Geology.* 87, 19–33.

Kruskal, W. H., and Wallis, W. A. (1952). Use of Ranks in One-Criterion Variance Analysis. *J. Am. Stat. Assoc.* 47, 583–621. doi:10.1080/01621459.1952.10483441

Lee, V. F. (1979). Maritime Pseudoscorpions of Baja California, Mexico (Arachnida: Pseudoscorpionida).

Mandeville, C. W., Carey, S., and Sigurdsson, H. (1996). Sedimentology of the Krakatau 1883 Submarine Pyroclastic Deposits. *Bull. Volcanol* 57, 512–529. doi:10.1007/BF00304436

Manville, V., Segschneider, B., and White, J. D. L. (2002). Hydrodynamic Behaviour of Taupo 1800a Pumice: Implications for the Sedimentology of Remobilized Pyroclasts. *Sedimentology* 49, 955–976. doi:10.1046/j.1365-3091.2002.00485.x

Matsumoto, H., Zampolli, M., Haralabus, G., Stanley, J., Mattila, J., and Meral Özel, N. (2019). Interpretation of Detections of Volcanic Activity at Ioto Island Obtained from *In Situ* Seismometers and Remote Hydrophones of the International Monitoring System. *Sci. Rep.* 9, 19519. doi:10.1038/s41598-019-55918-w

Mittal, T., and Delbridge, B. (2019). Detection of the 2012 Havre Submarine Eruption Plume Using Argo Floats and its Implications for Ocean Dynamics. *Earth Planet. Sci. Lett.* 511, 105–116. doi:10.1016/j.epsl.2019.01.035

Mouginis-Mark, P. J., and Zimbelman, J. R. (2020). Rafted Pumice: A New Model for the Formation of the Medusae Fossae Formation, Mars. *Icarus* 343, 113684. doi:10.1016/j.icarus.2020.113684

Ochoa, C. N. (2009). *Report of Drift Pumice Near Socorro Island (25 January to 3 February 2009)*.

O'Malley, R. T., Behrenfeld, M. J., Westberry, T. K., Milligan, A. J., Reese, D. C., and Halsey, K. H. (2014). Improbability Mapping: a Metric for Satellite-Detection of Submarine Volcanic Eruptions. *Remote sensing Environ.* 140, 596–603.

Osborne, N. M., Enright, N. J., and Parnell, K. E. (1991). The Age and Stratigraphic Significance of Sea-Rafted Loisels Pumice in Northern New Zealand. *J. R. Soc. New Zealand* 21, 357–371. doi:10.1080/03036758.1991.10420833

Park, C., and Schmincke, H.-U. (2020). Multistage Damming of the Rhine River by Tephra Fallout during the 12,900 Bp Plinian Laacher See Eruption (germany). Syn-Eruptive Rhine Damming I. *J. Volcanology Geothermal Res.* 389, 106688. doi:10.1016/j.jvolgeores.2019.106688

Planet Team (2021). "Planet Application Program Interface," in *Space for Life on Earth*.

Poland, M. P., Lopez, T., Wright, R., and Pavolonis, M. J. (2020). Forecasting, Detecting, and Tracking Volcanic Eruptions from Space. *Remote Sens Earth Syst. Sci.* 3, 55–94. doi:10.1007/s41976-020-00034-x

Pullar, W. A., Kohn, B. P., and Cox, J. E. (1977). Air-Fall Kaharoa Ash and Taupo Pumice, and Sea-Rafted Loisels Pumice, Taupo Pumice, and Leigh Pumice in Northern and Eastern Parts of the North Island, New Zealand. *New Zealand Journal Geology. Geophysics* 20, 697–717. doi:10.1080/00288306.1977.10430729

Qi, L., Hu, C., Mikelsons, K., Wang, M., Lance, V., Sun, S., et al. (2020). In Search of Floating Algae and Other Organisms in Global Oceans and Lakes. *Remote Sensing Environ.* 239, 111659. doi:10.1016/j.rse.2020.111659

Richards, A. F. (1958). Transpacific Distribution of Floating Pumice from Isla San Benedicto, Mexico. *Deep Sea Res. (1953)* 5, 29–35. doi:10.1016/S0146-6291(58)80005-3

Risso, C., Scasso, R. A., and Aparicio, A. (2002). Presence of Large Pumice Blocks on Tierra Del Fuego and South Shetland Islands Shorelines, From 1962 South Sandwich Islands Eruption. *Mar. Geology.* 186, 413–422. doi:10.1016/s0025-3227(02)00190-1

Rubin, K., Soule, S. A., Chadwick, W., Jr, Fornari, D., Clague, D., Embley, R., et al. (2012). Volcanic Eruptions in the Deep Sea. *oceanog* 25, 142–157. doi:10.5670/oceanog.2012.12

Sakuno, Y. (2021). Trial of Chemical Composition Estimation Related to Submarine Volcano Activity Using Discolored Seawater Color Data Obtained from GCOM-C SGLI. A Case Study of Nishinoshima Island, Japan, in 2020. *Water* 13, 1100. doi:10.3390/w13081100

Santana-Casiano, J. M., González-Dávila, M., Fraile-Nuez, E., De Armas, D., González, A. G., Domínguez-Yanes, J. F., et al. (2013). The Natural Ocean Acidification and Fertilization Event Caused by the Submarine Eruption of El Hierro. *Sci. Rep.* 3, 1140. doi:10.1038/srep01140

Scholz, F. W., and Stephens, M. A. (1987). K-Sample Anderson-Darling Tests. *J. Am. Stat. Assoc.* 82, 918–924. doi:10.1080/01621459.1987.10478517

Shane, P., Froggatt, P., Smith, I., and Gregory, M. (1998). Multiple Sources for Sea-Rafted Loisels Pumice, New Zealand. *Quat. Res.* 49, 271–279. doi:10.1006/qres.1998.1968

Tepp, G., Chadwick, W. W., Jr, Haney, M. M., Lyons, J. J., Dziak, R. P., Merle, S. G., et al. (2019). Hydroacoustic, Seismic, and Bathymetric Observations of the 2014 Submarine Eruption at Ahyi Seamount, Mariana Arc. *Geochem. Geophys. Geosyst.* 20, 3608–3627. doi:10.1029/2019gc008311

Tepp, G., and Dziak, R. P. (2021). The Seismo-Acoustics of Submarine Volcanic Eruptions. *J. Geophys. Res. Solid Earth* 126, e2020JB020912. doi:10.1029/2020jb020912

Thiel, M., and Gutow, L. (2004). The Ecology of Rafting in the Marine Environment. I. The Floating Substrata. *Oceanography Mar. Biol. Annu. Rev.* 42, 181–263. doi:10.1201/9780203507810.ch6

Tilstone, G. H., Miller, P. I., Brewin, R. J. W., and Priede, I. G. (2014). Enhancement of Primary Production in the North Atlantic Outside of the Spring Bloom, Identified by Remote Sensing of Ocean Colour and Temperature. *Remote sensing Environ.* 146, 77–86. doi:10.1016/j.rse.2013.04.021

Torres, R. C., Self, S., Martinez, M. M. L., Newhall, C., and Punongbayan, R. (1996). *Secondary Pyroclastic Flows from the June 15, 1991, Ignimbrite of Mount Pinatubo Fire and Mud: Eruptions and Lahars of Mount Pinatubo*. Philippines, 665–678.

White, J. D. L., Schipper, C. I., and Kano, K. (2015). "Submarine Explosive Eruptions," in *The Encyclopedia of Volcanoes*. Editor H. Sigurdsson. Second EditionSecond edition edn (Amsterdam: Academic Press), 553–569. doi:10.1016/B978-0-12-385938-9.00031-6

White, S. M., Crisp, J. A., and Spera, F. J. (2006). Long-term Volumetric Eruption Rates and Magma Budgets. *Geochem. Geophys. Geosystems* 7. doi:10.1029/2005gc001002

Whiteside, A., Dupouy, C., Singh, A., Frouin, R., Menkes, C., and Lefèvre, J. (2021). Automatic Detection of Optical Signatures within and Around Floating Tonga-Fiji Pumice Rafts Using MODIS, VIIRS, and OLCI Satellite Sensors. *Remote Sensing* 13, 501. doi:10.3390/rs13030501

Wilcock, W. S. D., Tolstoy, M., Waldhauser, F., Garcia, C., Tan, Y. J., Bohnenstiehl, D. R., et al. (2016). Seismic Constraints on Caldera Dynamics from the 2015 Axial Seamount Eruption. *Science* 354, 1395–1399. doi:10.1126/science.aah5563

Wright, R., Flynn, L. P., Garbeil, H., Harris, A. J. L., and Pilger, E. (2004). Modvolc: Near-Real-Time Thermal Monitoring of Global Volcanism. *J. Volcanology Geothermal Res.* 135, 29–49. doi:10.1016/j.jvolgeores.2003.12.008

Yoshida, K., Tamura, Y., Sato, T., Hanyu, T., Usui, Y., Chang, Q., et al. (2022). Variety of the Drift Pumice Clasts from the 2021 Fukutoku-Oka-no-Ba Eruption, Japan. *Isl. Arc* 31. doi:10.1111/iar.12441

Conflict of Interest: The authors declare that the research was conducted in the absence of any commercial or financial relationships that could be construed as a potential conflict of interest.